

# Proton conduction at the surface of Y-doped BaCeO<sub>3</sub> and its application to an air/fuel sensor

A. TOMITA, T. HIBINO\*

National Institute of Advanced Industrial Science and Technology (AIST), 2266-98 Anagahora, Shimoshidami, Moriyama-ku, Nagoya 463-8560, Japan  
E-mail: takashi.hibino@aist.go.jp

M. SUZUKI, M. SANO

Nagoya University, Furo-cho, Chikusa-ku, Nagoya 466-0804, Japan

25 mol% Y<sup>3+</sup>-doped BaCeO<sub>3</sub> (BCY25) showed an extremely low activation energy of 0.3 eV for proton conduction at the surface. The resulting overall conductivity at the surface reached  $8.24 \times 10^{-3} \text{ S cm}^{-1}$  at 400°C, which was 3, 8, and 28 times higher than those in the bulk of BCY25, 20 mol% Sm<sup>3+</sup>-doped ceria, and 8 mol% yttria-stabilized zirconia, respectively. Such fast proton conduction enabled an air/fuel (A/F) sensor using BCY25 as the solid electrolyte to work above 150°C for H<sub>2</sub> and above 250°C for C<sub>2</sub>H<sub>4</sub>. © 2004 Kluwer Academic Publishers

## 1. Introduction

The three-way catalyst efficiently eliminates pollutant emission in exhaust gases from gasoline engines at a stoichiometric air/fuel (A/F) ratio. The A/F ratio is monitored by using an A/F sensor, which exhibits a steep transition in the sensor output only when the stoichiometric combustion condition is satisfied. However, the conventional A/F sensors using yttria-stabilized zirconia (YSZ) electrolytes, become poor at operating temperatures below 500°C [1]. A key technology for the operation at reduced temperatures is the use of a highly ion-conductive electrolyte.

BaCeO<sub>3</sub> perovskite oxides exhibit proton conduction over the wide temperature range of 200 to 1000°C by substituting trivalent cations such as Y<sup>3+</sup>, Gd<sup>3+</sup> and Nd<sup>3+</sup> on some Ce<sup>4+</sup> sites [2–8]. Although several researchers had attempted to use doped BaCeO<sub>3</sub> materials as solid electrolytes for solid oxide fuel cells [8, 9–11], gas sensor [12, 13], and membrane reactors [14–16], they were unable to address advantages of these materials over traditional oxide-ion conductors such as YSZ and doped ceria, because the overall conductivities of the former were near or smaller than those of the latter under operating conditions ( $T = 600\text{--}1000^\circ\text{C}$ ). However, BaCeO<sub>3</sub> materials have the possibility that exhibit highly ion conductivities at reduced temperatures by the notion that proton conduction in the doped BaCeO<sub>3</sub> is governed by a mechanism based on the hopping of an extremely small proton between adjacent oxide ions [3, 4, 6–8]. This results in lower activation energies for proton conduction than those for oxide-ion conduction in YSZ and the doped ceria.

In this study, we focused on the improvement of proton conduction not only in the bulk of Y<sup>3+</sup>-doped

BaCeO<sub>3</sub> (BCY) but also at its surface. As a result, it is found that the BCY showed significantly high proton conductivities at the surface. Furthermore, it is demonstrated that an A/F sensor using surface conduction of the BCY worked at reduced temperatures between 150 and 250°C.

## 2. Experimental procedure

### 2.1. BCY electrolytes

The BCY electrolytes used in this study were prepared as follows. The desired amounts of Ba(CH<sub>3</sub>COO)<sub>2</sub> (99.9%, Wako), CeO<sub>2</sub> (99.9%, Wako), and Y<sub>2</sub>O<sub>3</sub> (99.99%, Koch) powders were mixed in ethanol with a mortar and a pestle and then calcined in air at 1500°C for 10 h. The compound was ground in ethanol using a planetary ball mill (Fritsch P-5) with a zirconia mill container and zirconia balls at 180 r.p.m. for 14 h. The crystalline structure of the powders was examined by XRD analysis (Rigaku Rotaflex). The powder was hydrostatically pressed into a pellet at  $2 \times 10^3 \text{ kg cm}^{-2}$  and then sintered at 1675°C in air for 12 h. After cutting of the pellet into disks with appropriate dimensions for measurements of their conductivity and sensing properties, the disk surface was polished using abrasive papers with different mean particle sizes (3.0–58.5 μm) in order to prepare various surface morphologies, which were determined using a roughness tester. YSZ and Ce<sub>0.8</sub>Sm<sub>0.2</sub>O<sub>1.9</sub> (SDC) electrolytes were also used for comparison.

### 2.2. Conductivity measurement

Conductivity measurements for the test specimens were carried out using two Pt electrodes with the different

\*Author to whom all correspondence should be addressed.

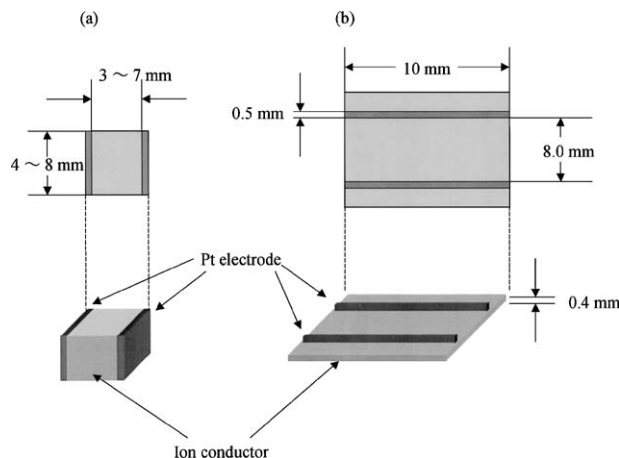


Figure 1 Schematic illustrations of two electrode configurations for conductivity measurements. Two Pt electrodes were placed on opposite surfaces (a) and the same surface (b) of BCY, SDC, or YSZ.

configurations shown in Fig. 1a and b. A commercial Pt paste (Tokuriki) was diluted with ethyl carbitol and then smeared as thinly as possible with a brush on the opposite surfaces or the same surface of the electrolyte. All the smeared electrodes were baked at 900°C in air for 1 h. An Au mesh and two Au wires served as the electrical collector and the output terminals, respectively, for each electrode. The specimens were pretreated under measuring conditions at 800°C for a few hours: the BCY was supplied with H<sub>2</sub> gas saturated with H<sub>2</sub>O vapor at room temperature or with D<sub>2</sub> gas similarly treated with D<sub>2</sub>O vapor at a flow rate of 50 ml min<sup>-1</sup>, and the other specimens were exposed to atmospheric air. The conductivities were evaluated from a.c. impedance spectra (1 Hz–100 kHz) between 400 and 800°C.

### 2.3. EMF measurement using air/fuel sensor

Electromotive force (EMF) measurements for an electrochemical cell using the BCY electrolyte was made using the Pt and Au electrodes with the configuration shown in Fig. 2, where the shortest gap between the electrodes was 0.5 mm. The Au mesh and the Au wire similarly served as the current collector and the output terminal, respectively. The cell was supplied with flowing mixture of H<sub>2</sub>, C<sub>2</sub>H<sub>6</sub>, C<sub>2</sub>H<sub>4</sub> or C<sub>2</sub>H<sub>2</sub>, and O<sub>2</sub> in argon saturated with H<sub>2</sub>O vapor at room temperature at a flow rate of 50 ml min<sup>-1</sup> between 150 and 400°C: the H<sub>2</sub> concentration was changed from 0 to 800 ppm while the O<sub>2</sub> concentration was maintained at 300 ppm: the C<sub>2</sub>H<sub>6</sub>, C<sub>2</sub>H<sub>4</sub> or C<sub>2</sub>H<sub>2</sub> concentration was changed from 0 to 600 ppm while the O<sub>2</sub> concentration was maintained at 1000 ppm. The EMF value was measured by an electrometer (Hokuto Denko HE-104) with a portable recorder (Yokogawa 3057).

### 2.4. Catalytic activity measurement

Catalytic activity measurements for the Pt and Au electrodes were performed by feeding a mixture of H<sub>2</sub>, C<sub>2</sub>H<sub>6</sub>, C<sub>2</sub>H<sub>4</sub> or C<sub>2</sub>H<sub>2</sub> and O<sub>2</sub> in argon saturated with H<sub>2</sub>O vapor at room temperature at a flow rate of 50 ml

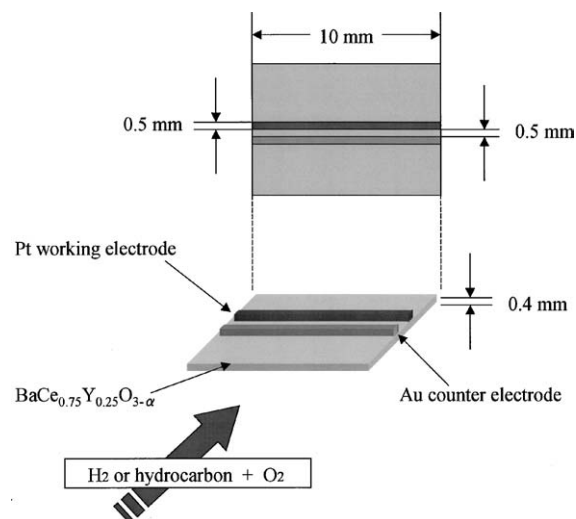


Figure 2 Schematic illustrations of two electrode configurations for EMF measurements. Pt and Au electrodes were attached on the same surface of BCY25.

min<sup>-1</sup> at 300°C into the specimen with the Pt or Au electrode. The outlet gas from the specimen was analyzed by two on-line gas chromatographs (Shimadzu GC-8A for separation of H<sub>2</sub> and CHROMPACK CP-2002 for separation of C<sub>2</sub>H<sub>6</sub> and C<sub>2</sub>H<sub>4</sub>).

## 3. Results and discussion

### 3.1. Proton conduction in BCY electrolytes

The Y<sup>3+</sup>-doped BaCeO<sub>3</sub> reported thus far showed the highest overall conductivities at Y<sup>3+</sup> = 20 mol%, since this was a critical solubility at calcining temperatures below 1450°C [17, 18]. However, as shown in Fig. 3, a rise in the calcining temperature to 1500°C permitted the formation of a single perovskite phase even at Y<sup>3+</sup> = 30 mol%: there were only peaks assigned to the perovskite phase in the XRD pattern after calcination at 1500°C, below which other peaks, mainly assigned to Y<sub>2</sub>O<sub>3</sub>, were included. Fig. 4 shows the conductivities of BCY (Y<sup>3+</sup> = 10–30 mol%) in H<sub>2</sub> gas saturated with H<sub>2</sub>O vapor at room temperature together with those of YSZ and Ce<sub>0.8</sub>Sm<sub>0.2</sub>O<sub>1.9</sub> (SDC) in atmospheric air. It was found that 25 mol% Y<sup>3+</sup>-doped BCY (BCY25) exhibited the highest conductivities between 400 and 800°C, which were about 1.2–1.6 times higher than those of 20 mol% Y<sup>3+</sup>-doped BCY. Furthermore, the

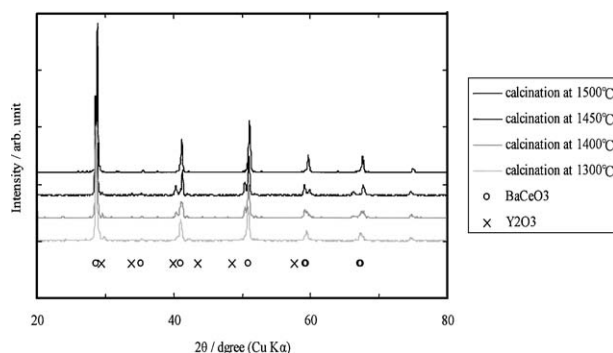


Figure 3 X-ray powder diffraction patterns of BaCe<sub>0.75</sub>Y<sub>0.25</sub>O<sub>3-α</sub>.

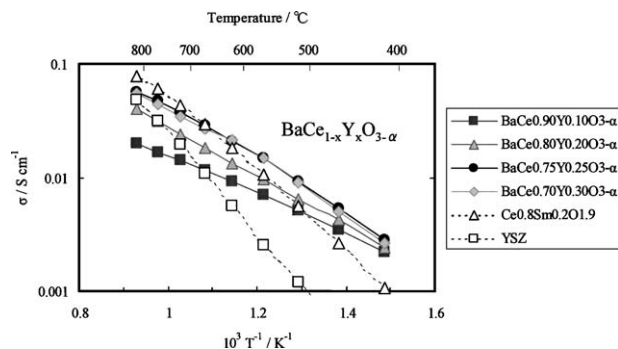


Figure 4 Temperature dependences of overall conductivities in  $\text{BaCe}_{1-x}\text{Y}_x\text{O}_{3-\alpha}$  ( $0.10 \leq x \leq 0.30$ ), SDC, and YSZ with electrode configurations shown in Fig. 1a.

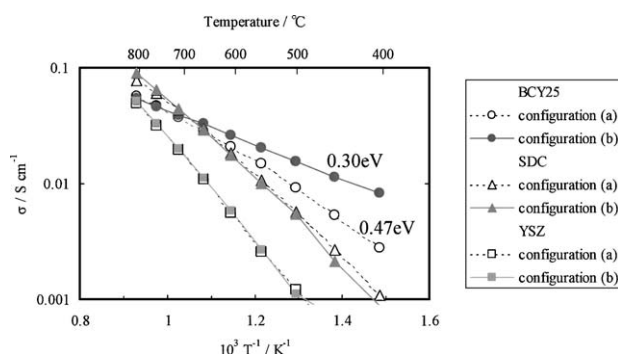


Figure 5 Temperature dependences of overall conductivities in BCY25, SDC, and YSZ with electrode configurations shown in Fig. 1a and b.

conductivities of BCY25 were characterized by comparison with the conductivities of YSZ and SDC as follows. The conductivities of the three ion conductors were in the order of  $\text{SDC} > \text{BCY25} > \text{YSZ}$  above  $600^\circ\text{C}$ ;  $\text{SDC} = \text{BCY25} > \text{YSZ}$  at  $600^\circ\text{C}$ ;  $\text{BCY25} > \text{SDC} > \text{YSZ}$  below  $600^\circ\text{C}$ .

Fig. 5 shows the overall conductivities of the three ion conductors, each of which have the two electrode configurations shown in Fig. 1a and b. The conductivities of the ion conductors with the configuration shown in Fig. 1b were calculated using the formula,

$$\sigma = R^{-1} \cdot l / (a \cdot b) \quad (1)$$

where  $l$  is the distance between the two electrodes,  $a$  is the length of the electrodes, and  $b$  is the electrolyte thickness. The YSZ and the SDC showed conductivities almost independent of the difference in electrode configuration, whereas the BCY25 exhibited enhanced conductivities when the two electrodes were placed on the same surface of the specimen. In addition, the apparent activation energy for conduction was reduced from 0.47 to 0.30 eV. The resulting conductivity of the BCY25 with the electrode configuration shown in Fig. 1b reached  $8.24 \times 10^{-3} \text{ S cm}^{-1}$  at  $400^\circ\text{C}$ , which was comparable to those of the SDC at  $550^\circ\text{C}$  and of the YSZ at  $650^\circ\text{C}$ . Although almost all charge carriers conduct through the BCY25 bulk in the electrode arrangement shown in Fig. 1a, a fraction of charge carrier passes along the BCY25 surface in the electrode arrangement shown in Fig. 1b. In particular, the relatively larger distance between the two electrodes

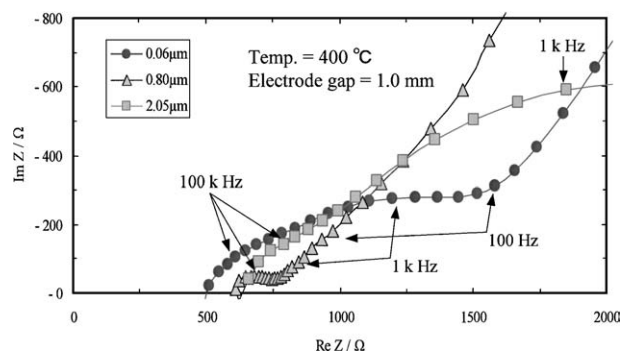


Figure 6 Impedance spectra of BCY25 with different surface morphologies using the electrode configuration shown in Fig. 1b in  $\text{H}_2$  gas saturated with  $\text{H}_2\text{O}$  vapor at room temperature operating at  $400^\circ\text{C}$ : Surface roughnesses were 0.06, 0.80, and  $2.05 \mu\text{m}$ .

(8.0 mm) compared to the thickness of the specimen (0.4 mm) suggests that surface conduction would make some contribution to the observed conductivity.

Evidence for the above suggestion is provided by the impedance spectra of the BCY25 with different surface morphologies at  $400^\circ\text{C}$  (Fig. 6): the resistance of the BCY25 with the electrode configuration shown in Fig. 1b were 25, 30, and  $32 \Omega \text{ cm}^2$  at surface roughnesses of 0.06, 0.80, and  $2.05 \mu\text{m}$ , respectively. This also offers the notion that there is an additional fast pathway of charge carriers at the BCY25 surface, which is strongly sensitive to the surface morphology. We, of course, confirmed that the resistances of the YSZ and the SDC with the electrode configuration shown in Fig. 1b were not at all affected by the change in surface morphology.

Determination of the species migrating at the BCY25 surface is necessary in order to better understand the above results. Protons and hydroxide ions are general candidates for defects in proton-conducting oxides operating at elevated temperatures, but conduction of oxide ions and electron holes is also possible in the doped  $\text{BaCeO}_3$ . An H/D isotope effect would give information about this point [3–5]. As shown in Fig. 7, the BCY25 with the electrode configuration shown in Fig. 1b presented a large H/D isotope effect with a difference in activation energy of about 0.066 eV. This provides primary evidence that the oxide ions and the electron holes are not the dominant defects. A similar conclusion can

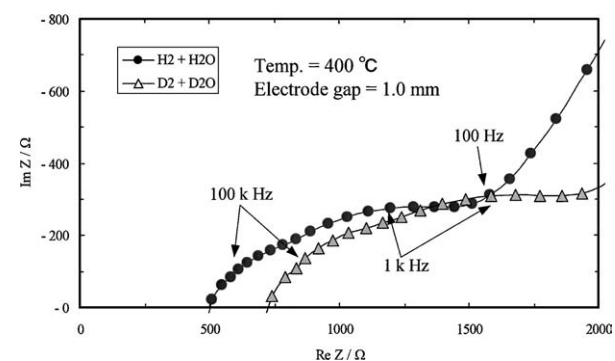


Figure 7 Impedance spectra of BCY25 with electrode configuration shown in Fig. 1b in  $\text{H}_2$  gas saturated with  $\text{H}_2\text{O}$  vapor and in  $\text{D}_2$  gas saturated with  $\text{D}_2\text{O}$  vapor.

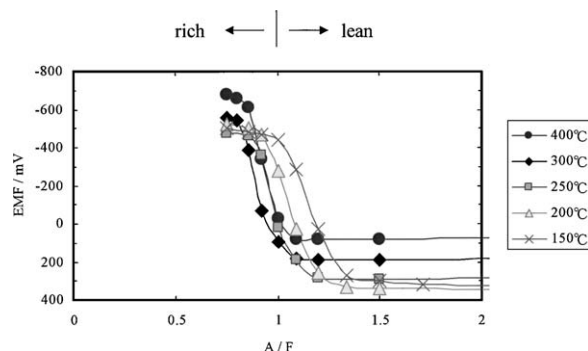
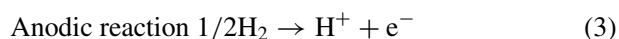
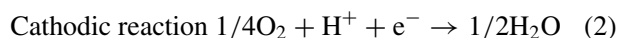


Figure 8 EMFs of air/fuel sensor using BCY25 electrolyte with the electrode configuration shown in Fig. 2 in a mixture of 0–800 ppm H<sub>2</sub> and 300 ppm O<sub>2</sub> in argon saturated with H<sub>2</sub>O vapor at room temperature operating at 200–400°C.

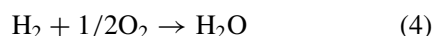
also apply to the hydroxide ions, because of the small 17:18 mass ratio of OH and OD. It is clear that the protons migrate by jumping between the adjacent oxide ions at the BCY25 surface.

### 3.2. Air/fuel sensor

We fabricated a simple *A/F* sensor using the Pt working and Au counter electrodes with the electrode configuration shown in Fig. 2. The EMF measurement was carried out by feeding a mixture of 0–800 ppm H<sub>2</sub> and 300 ppm O<sub>2</sub> in argon saturated with H<sub>2</sub>O vapor at room temperature into the sensor between 150 and 400°C. As shown in Fig. 8, the EMF generated from the sensor remarkably changed near a stoichiometric point (*A/F* = 1) throughout the tested temperature range, where the potential of the Pt electrode was negative against the Au electrode under rich conditions (*A/F* < 1) and positive under lean conditions (*A/F* > 1). We note that the excellent performance of this sensor at low operating temperature was due to the high conductivity at the BCY25 surface. We also explained the change in EMF with the *A/F* ratio shown in Fig. 8 using a mechanism of the mixed potential as below. When the electrode is exposed to the mixture of H<sub>2</sub> and O<sub>2</sub>, the following electrode reactions would proceed at the same time:



The electrode show a mixed potential based on Equations 2 and 3, where the mixed potential becomes more negative as the electrode favors reaction (3) rather than reaction (2). From the analysis of the outlet gas from the cell having only the Pt or Au electrode (Table I(a)), it was found that under lean conditions, 93% of total H<sub>2</sub> gas was completely oxidized by O<sub>2</sub> to form H<sub>2</sub>O vapor over the Pt electrode as below,



while this reaction proceeded at a very slow rate over the Au electrode. Therefore, since the mixed potential of the Pt electrode is more significantly dependent on reaction (2) than that of the Au electrode, the potential

TABLE I Compositions of inlet and outlet gases from working chamber with Pt or Au electrode at 300°C: using a flowing mixture of H<sub>2</sub>, C<sub>2</sub>H<sub>6</sub>, C<sub>2</sub>H<sub>4</sub> or C<sub>2</sub>H<sub>2</sub> and O<sub>2</sub> in argon saturated with H<sub>2</sub>O vapor at room temperature at a flow rate of 50 ml min<sup>-1</sup>: (a) *x* ppm H<sub>2</sub> and 300 ppm O<sub>2</sub>, (b) *x* ppm C<sub>2</sub>H<sub>6</sub> and 1000 ppm O<sub>2</sub>, (c) *x* ppm C<sub>2</sub>H<sub>4</sub> and 1000 ppm O<sub>2</sub>, (d) *x* ppm C<sub>2</sub>H<sub>2</sub> and 1000 ppm O<sub>2</sub>.

	Inlet gas (ppm)		Outlet gas (ppm)			
			Pt electrode		Au electrode	
	H <sub>2</sub>	O <sub>2</sub>	H <sub>2</sub>	O <sub>2</sub>	H <sub>2</sub>	O <sub>2</sub>
(a)						
Lean	300	300	20	198	300	300
Stoichiometric	600	300	34	124	600	300
Rich	900	300	140	60	900	300
(b)						
	C <sub>2</sub> H <sub>6</sub>	O <sub>2</sub>	C <sub>2</sub> H <sub>6</sub>	O <sub>2</sub>	C <sub>2</sub> H <sub>6</sub>	O <sub>2</sub>
Lean	150	1000	150	1000	150	1000
Stoichiometric	286	1000	286	1000	286	1000
Rich	400	1000	400	1000	400	1000
(c)						
	C <sub>2</sub> H <sub>4</sub>	O <sub>2</sub>	C <sub>2</sub> H <sub>4</sub>	O <sub>2</sub>	C <sub>2</sub> H <sub>4</sub>	O <sub>2</sub>
Lean	200	1000	76	678	200	1000
Stoichiometric	333	1000	158	604	333	1000
Rich	500	1000	264	486	500	1000
(d)						
	C <sub>2</sub> H <sub>2</sub>	O <sub>2</sub>	C <sub>2</sub> H <sub>2</sub>	O <sub>2</sub>	C <sub>2</sub> H <sub>2</sub>	O <sub>2</sub>
Lean	300	1000	191	764	300	1000
Stoichiometric	400	1000	301	834	400	1000
Rich	500	1000	385	792	500	1000

of the Pt electrode is positive against the Au electrode. On the other hand, under rich conditions, almost all the O<sub>2</sub> was consumed for reaction (4) over the Pt electrode, while this reaction was inhibited over the Au electrode (Table I(a)). The lower O<sub>2</sub> concentration at the Pt electrode than that at the Au electrode depressed reaction (2), thus resulting in a more negative potential of the Pt electrode than that of the Au electrode.

Furthermore, the present sensor was examined for hydrocarbons. We previously reported that the Pt electrode also shows a large mixed potential based on Equations 2 and 5 in a mixture of hydrocarbon and O<sub>2</sub> [19]:



Fig. 9 shows the EMF of the sensor for C<sub>2</sub> hydrocarbons (C<sub>2</sub>H<sub>6</sub>, C<sub>2</sub>H<sub>4</sub> and C<sub>2</sub>H<sub>2</sub>) at 300°C. The change in EMF for C<sub>2</sub>H<sub>4</sub> and C<sub>2</sub>H<sub>2</sub> with the *A/F* ratio was similar to that observed for H<sub>2</sub>. This can be explained by the difference in catalytic activity for the combustion of C<sub>2</sub>H<sub>4</sub> and C<sub>2</sub>H<sub>2</sub> between the two electrodes as described in the preceding paragraph: C<sub>2</sub>H<sub>4</sub> and C<sub>2</sub>H<sub>2</sub> more burned over the Pt electrode than over the Au electrode (Table I(c) and (d)). However, the sensor had no response to C<sub>2</sub>H<sub>6</sub> at all the *A/F* ratio (Fig. 9). The oxidation rate of C<sub>2</sub>H<sub>6</sub> was too slow to cause a large difference in both C<sub>2</sub>H<sub>6</sub> and O<sub>2</sub> concentrations between the two electrodes (Table I(b)).

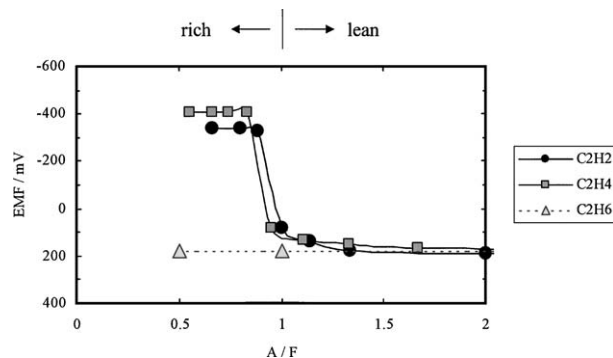


Figure 9 EMFs of air/fuel sensor using BCY25 electrolyte with the electrode configuration shown in Fig. 2 in a mixture of 0–600 ppm C<sub>2</sub>H<sub>6</sub>, C<sub>2</sub>H<sub>4</sub>, or C<sub>2</sub>H<sub>2</sub> and 1000 ppm O<sub>2</sub> in argon saturated with H<sub>2</sub>O vapor at room temperature operating at 300°C.

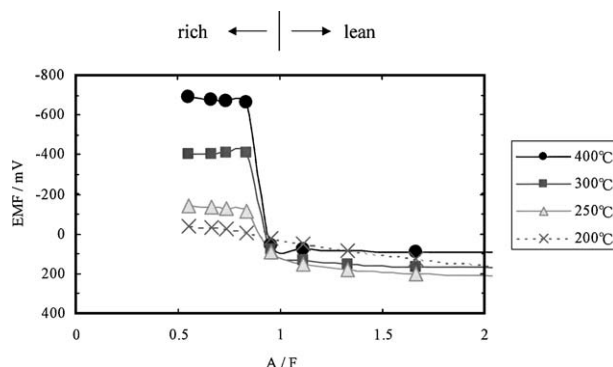


Figure 10 EMFs of air/fuel sensor using BCY25 electrolyte with the electrode configuration shown in Fig. 2 in a mixture of 0–600 ppm C<sub>2</sub>H<sub>4</sub> and 1000 ppm O<sub>2</sub> in argon saturated with H<sub>2</sub>O vapor at room temperature operating at 200–400°C.

The temperature dependence of the EMF generated from the sensor was investigated for C<sub>2</sub>H<sub>4</sub> between 200 and 400°C (Fig. 10). The sensor worked as an A/F sensor above 250°C but showed little sensitivity to C<sub>2</sub>H<sub>4</sub> below 250°C. This was due to the fact that C<sub>2</sub>H<sub>4</sub> remained unreacted over the Pt electrode below 250°C. Thus, the use of a more catalytically active electrode for the oxidation of hydrocarbons than the Pt electrode is required for fabrication of the A/F sensor for hydrocarbons below 250°C.

The present sensor exhibited the excellent sensing properties for H<sub>2</sub> above 150°C and for C<sub>2</sub>H<sub>4</sub> above 250°C. However, Scholten et al. have pointed out that BaCeO<sub>3</sub>-based oxides react with gaseous CO<sub>2</sub> to form BaCO<sub>3</sub> and CeO<sub>2</sub> [6]. Although this reaction thermodynamically occurs below 1200°C [9], it would be kinetically inhibited under the present condition such as below 400°C. We will demonstrate the long-term stability of the present sensor in the future.

## 4. Conclusions

The Y<sup>3+</sup>-doped BaCeO<sub>3</sub> exhibited the highest ion conductivity at Y<sup>3+</sup> = 25 mol%, which was allowed to be a single perovskite phase by calcination at 1500°C. In addition, ion conductivity of this material at the surface was higher than that in the bulk. The resulting overall conductivity at the surface reached  $8.24 \times 10^{-3} \text{ S cm}^{-1}$  at 400°C, which was 8 and 28 times higher than those in the bulk of 20 mol% Sm<sup>3+</sup>-doped ceria, and 8 mol% yttria-stabilized zirconia, respectively. Such high proton conductivity enabled the A/F sensor using the BCY 25 electrolyte to exhibit the excellent sensing properties for H<sub>2</sub> above 150°C and for C<sub>2</sub>H<sub>4</sub> above 250°C.

## Acknowledgment

The authors are grateful to Professor H. Iwahara of Nagoya University for technical advice.

## References

1. W. J. FLEMING, *J. Electrochem. Soc.* **124** (1977) 21.
2. N. BONANOS, B. ELLIS, K. S. KNIGHT and M. N. MAHMOOD, *Solid State Ionics* **35** (1989) 179.
3. T. NORBY, *ibid.* **40/41** (1990) 857.
4. R. C. T. SLADE and N. SINGH, *J. Mater. Chem.* **1** (1991) 441.
5. J. F. LIU and A. S. NOWICK, *Solid State Ionics* **50** (1992) 131.
6. M. J. SCHOLTEN, J. SCHOONMAN, J. C. VAN MILTENBURG and H. A. J. OONK, *ibid.* **61** (1993) 83.
7. T. HE, K. D. KREUER, YU. M. BAIKOV and J. MAIER, *ibid.* **95** (1997) 301.
8. H. IWAHARA, T. YAJIMA, T. HIBINO and H. USHIDA, *J. Electrochem. Soc.* **140** (1993) 1687.
9. N. BONANOS, B. ELLIS and M. N. MAHMOOD, *Solid State Ionics* **44** (1991) 305.
10. Y. DU and A. S. NOWICK, *ibid.* **91** (1996) 85.
11. T. SCHÖBER, F. KRUG and W. SCHILLING, *ibid.* **97** (1997) 369.
12. T. HIBINO and H. IWAHARA, *Chem. Lett.* (1992) 1225.
13. N. TANIGUCHI, E. YASUMOTO, Y. NAKAGIRI and T. GAMO, *J. Electrochem. Soc.* **145** (1998) 1744.
14. J. GUAN, S. E. DORRIS, U. BALACHANDRAN and M. LIU, *Solid State Ionics* **100** (1997) 45.
15. T. HIBINO, K. USHIKI and Y. KUWAHARA, *J. Chem. Soc., Chem. Commun.* (1995) 1001.
16. G. MARNELLOS and M. STOUKIDES, *Science* **282** (1998) 98.
17. H. IWAHARA, *Solid State Ionics* **77** (1995) 289.
18. J. GUAN, S. E. DORRIS, U. BALACHANDRAN and M. LIU, *J. Electrochem. Soc.* **145** (1998) 1780.
19. T. HIBINO, A. HASHIMOTO, K. MORI and M. SANO, *J. Phys. Chem. B* **105** (2001) 10648.

Received 23 July 2002

and accepted 24 November 2003